International Journal of Nanomedicine

Dovepress
open access to scientific and medical research

Open Access Full Text Article

ORIGINAL RESEARCH

Osteoclast-Derived Exosomal miR-5134-5p Interferes with Alveolar Bone Homeostasis by Targeting the JAK2/STAT3 Axis

Lai Pan*, Chenyi Zhang*, Haizheng Zhang, Ting Ke, Mengyao Bian, Yuxuan Yang, Lili Chen, Jingyi Tan

Department of Periodontology, The Second Affiliated Hospital of Zhejiang University, School of Medicine, Hangzhou, 310009, People's Republic of China

*These authors contributed equally to this work

Correspondence: Jingyi Tan; Lili Chen, Email tanjingyi@zju.edu.cn; chenlili_1030@zju.edu.cn

Background: In chronic periodontitis, exosomes transport various informative substances between osteoclasts and osteoblasts in alveolar bone. Herein, we aimed to investigate the effect of exosomal micro-ribonucleic acid (miRNA/miR)-5134-5p derived from osteoclasts on osteoblastic proliferation and differentiation and the development of periodontitis in vivo and in vitro.

Methods: The effects of OC-Exos on the proliferation and differentiation of osteoblasts were identified by Real-time quantitative reverse polymerase chain reaction (qRT-PCR), Western blot(WB), alkaline phosphatase(ALP) staining, etc. Exosomal miRNA expression was analyzed by sequencing. The sites of miRNA action were predicted through TargetScan and tested by double luciferase assay. After transfecting miR-5134-5p mimic/inhibitor into osteoblasts, we measured the proliferation and differentiation of osteoblasts by ALP staining and WB, etc. Furthermore, OC-Exos were injected into the gingival sulcus at the ligation site. Inflammation was observed by Hematoxylin-eosin (H&E) staining, the expression of inflammatory factors were detected by qRT-PCR, the resorption of alveolar bone was observed by Micro CT.

Results: Osteoblastic proliferation and differentiation were negatively regulated by OC-Exos in vitro. miRNA sequencing analysis revealed that miR-5134-5p expression was significantly elevated in OC-Exos, which also increased in osteoblasts following OC-Exo intervention. The dual-luciferase assay revealed that miR-5134-5p and Janus kinase 2 (JAK2) had binding sites. miR-5134-5p-mimics could upregulate miR-5134-5p expression in osteoblasts while downregulating Runt-related transcription factor 2(Runx2), phosphorylated-JAK2 (p-JAK2), and phosphorylated-signal transducer and activator of transcription 3 (p-STAT3) expression and inhibited osteogenic differentiation. However, miR-5134-5p-inhibitor had the opposite effect. In vivo, the OC-Exo group demonstrated morphological disruption of periodontal tissue, massive inflammatory cell infiltration, upregulation of inflammatory factors mRNA expression, a significant decrease in BV/TV, and an increase in the cementoenamel junction and alveolar bone crest distance.

Conclusion: Osteoclast-derived exosomal miR-5134-5p inhibits osteoblastic proliferation and differentiation via the JAK2/STAT3 pathway. OC-Exos exacerbate periodontal tissue inflammation and accelerate alveolar bone resorption in mice with experimental periodontitis.

Keywords: exosomes, miR-5134-5p, bone homeostasis, JAK2/STAT3 pathway, osteoclast-osteoblast communication

Introduction

Periodontitis is a chronic infectious disease characterized by progressive alveolar bone resorption. Alveolar bone loss occurs because of inflammatory responses triggered by bacteria and their products.[1]

The two basic functional cells of bone metabolism, osteoclasts, and osteoblasts, dominate the balanced dynamic process of bone resorption and formation.[2] This balance gets disturbed as periodontitis progresses. The paracrine pathway plays a crucial role in the communication between osteoblasts and osteoclasts, wherein exosomes serve as representative members. Exosomes are the membrane-bound vesicles produced in intracellular multivesicular bodies and are released into the extracellular matrix. Previous studies have reported that osteoblasts regulate bone resorption via

Received: 22 March 2023
Accepted: 30 June 2023
Published: 7 July 2023

exosomes targeting osteoclasts.[3–5] However, osteoclast-to-osteoblast crosstalk by exosomes in periodontitis lacks research.

Micro-ribonucleic acids (RNAs) (miRNAs/miRs) are non-coding single-stranded RNAs comprising approximately 22 nucleotides that can identify and band to the 3'-untranslated region of target messenger RNAs (mRNAs) and reverse their expression by incomplete base pairing.[6–9] However, miRNAs are susceptible to degradation owing to their instability in the extracellular space. The exosomes incorporate, transfer, stabilize, and protect themselves from degradation.[10–12] Lv et al[13] found that miR-181b-5p delivered by osteocyte-derived exosomes promotes human periodontal ligament stem cell proliferation via the phosphatase and tensin homolog(PTEN)/protein kinase B(PKB) pathway, suggesting that miRNA-carrying exosomes are crucial for bone remodeling in periodontitis.[14,15] Hu et al[3] illustrated that sympathetic neuro-stress could drive osteoblastic exosomal miR-21 transfer to regulate osteoclastogenesis. However, the exact miRNAs that aid in intercellular signaling during the exchange between osteoclasts and osteoblasts via exosomes in periodontitis and the underlying specific mechanisms remain unclear.

In this study, we aimed to investigate whether osteoclasts can interfere with osteoblastic proliferation and differentiation by secreting miRNA-carrying exosomes and identify the role of OC-Exos in periodontitis progression. According to our findings, our study was the first to report that miR-5134-5p is highly expressed in mature osteoclast exosomes, which could be secreted during bone resorption in mature osteoblasts. miR-5134-5p transported in OC-Exos could silence the JAK 2/STAT 3 pathway to inhibit the transcriptional activity of Runx2 and alter osteoblastic differentiation in vitro. OC-Exos promoted periodontal inflammatory response and accelerated alveolar bone destruction in vivo.

Methods

Isolating and Cultivating Cells

RAW264.7 and MC3T3-E1 cells were procured from the National Collection of Authenticated Cell Cultures (Shanghai, China). Osteoblasts were enzymatically isolated from the skull bones of 1-day-old C57BL/6 mice.[16] RAW264.7 cells were cultured in Dulbecco's Modified Eagle Medium (DMEM) (Sigma, USA) supplemented with 100 U/μL penicillin, streptomycin (TBD Science, China), and 10% fetal bovine serum (FBS) (Bovogen, AUS). Osteoblastic and MC3T3-E1 cells were cultured in DMEM (Kaiji, China) supplemented with 10% FBS (Every Green, China), 100 U/μL penicillin, and 100 U/μL streptomycin. The cells were incubated under 5% carbon dioxide (CO_2) at 37°C until 70–80% convergence was reached.

Differentiation of Osteoblasts and Staining with Alizarin Red and Alkaline Phosphatase (ALP)

The osteogenic induction medium (Ind) comprising the above-mentioned control medium, 10 nM dexamethasone (Sigma, USA), 10 mM β-glycerophosphate (Sigma, USA), and 50 μg/mL l-ascorbic acid (Sigma, USA). A 5-bromo-4-chloro-3-indolyl phosphate/nitro blue tetrazolium ALP color development kit (Beyotime, China) was used to develop the color of the osteoblasts 7 days after osteogenic induction. Osteoblast-like cells were detected by Alizarin red staining (FDbio, China). Image acquisitions and observations were performed using an inverted microscope (Solms, Germany). Each experiment was performed in triplicate.

Differentiation of Osteoclasts and Staining with Tartrate-Resistant Acid Phosphatase (TRAP)

α-minimum essential medium (MEM) (Gibco, USA) comprising 1% penicillin-streptomycin, 10% FBS, and 50 ng/mL receptor activator of nuclear factor kappa-B ligand (RANKL) (Novoprotein, China) was used to induce RAW264.7 cells for 5 days. The medium was changed every 2 days, and the TRAP staining kit (Sigma-Aldrich, USA) was used to stain the TRAP in the osteoclasts after the formation of mature osteoclasts. An osteoclast having three or more nuclei was considered mature if it was TRAP-positive. Inverted microscopy was used to measure and score the number and size of the mature osteoclasts.

Purification of Exosomes

After 5 days of RANKL (50 ng/mL) induction, osteoclasts were cultured with a medium comprising exosome-free FBS. After a 48-h culture, dead cells and debris from cellular supernatants were discarded by centrifuging at 3000 ×g for 10 min. A 70-min ultracentrifugation at 110,000 ×g at 4°C was performed on the supernatants. After resuspension in phosphate-buffered saline (PBS), the precipitate was further centrifuged for 70 min at 110,000 ×g. The precipitate was dissolved in 100 μL of PBS to form a final precipitate (exosomes), which was stored at −80°C.

Characterization of Exosomes

Transmission electron microscopy (TEM; Tecnai G2 Spirit, FEI, USA) was used to examine the OC-Exos. The copper grids were stained using 2% phosphotungstic acid after being incubated with an adequate amount of exosomal solution for 5 min at 37°C. TEM was used to observe and photograph the exosomes when the grids were dry. A dilution of 500 ng/mL of collected OC-Exos was used to avoid interparticle interactions. Exosomal size distribution was analyzed using NS300 (NanoSight, UK).

PKH67-Labelled Exosomes Internalize in vitro

PKH67 (Sigma, USA) was used as a labeling agent to evaluate if OC-Exos can be absorbed by osteoblasts. PKH67 was incubated for 10 min, followed by centrifugation for 90 min at 120,000 ×g to collect exosomes. These exosomes were then added to the osteoblastic cells culture medium, where they were incubated for 12 h. Phalloidin and 4′,6-diamidino-2-phenylindole (Beyotime, China) were used to stain the nucleus and the osteoblasts with F-actin. A confocal microscope (Zeiss, Germany) was used to record the images.

Cell Viability Assay (Cell Counting Kit-8 [CCK-8])

Cell proliferation was measured using the CCK-8 (Yeason, China). The osteoblasts were cultured in a 96-well plate (5×10^3 cells/well) and were subjected to the following treatments: Ind and OC-Exos (20 μg/mL, 50 μg/mL, and 80 μg/mL). The optical density was measured after 48 h at a wavelength of 450 nm using a microplate reader (Bio-Rad, USA).

Osteoblastogenesis Co-Culture Assay

Well inserts with a 0.4-μm pore-sized filter (Corning, USA) were used as per the manufacturer's instructions. Induced osteoclasts from RAW264.7 cells were seeded into six-well plates with complete α-MEM containing RANKL. Osteoblasts were seeded into the well inserts and differentiated with Ind. A 5-day co-culture was performed after differentiating the osteoblasts and osteoclasts.

Construction of Complementary Deoxyribonucleic Acid (DNA) (cDNA) Libraries and mRNA Sequencing

The experimental procedures, including the preparation of the libraries and sequencing, were performed according to the instructions provided by Illumina (Illumina, USA). A small RNA library preparation kit (TruSeq Small RNA Library Prep Kit, Illumina, USA) was used to create the sequencing libraries. The purified library products were sequenced using Illumina Hiseq 2000/2500 (the 1×50 bp mode).

The miRNA data analysis software ACGT101-mir (LC Sciences, USA) was used. This software performs the analysis as follows: (1) data cleaning: by removing 3' connections and garbage sequences; (2) the length screening should be performed on sequences whose bases range between 18 and 26 nucleotides; (3) comparison and analysis of various RNA databases conducted using the remaining sequences (excluding miRNA) and filtering against the mRNA, RFam, and Repbase databases; (4) identification of miRNA: miRNA is identified by comparing the precursor and genome data; (5) miRNA difference analysis.

All sequencing data are publicly available to GEO database (GSE222004).

Target Gene Prediction and Dual-Luciferase Reporter Assay

miR-5134-5p's potential molecular targets were predicted through http://www.targetscan.org (TargetScan 4.2). As a potential target, we focused on JAK2, which is part of the JAK/STAT pathway that plays a significant role in osteoblastic differentiation and bone formation.[14,15]

A conventional method was used to construct wild-type (WT)-JAK2 plasmids fused with luciferase genes and mutant (MUT) JAK2 fusion genes. The logarithmic growth phase of MC3T3-E1 cells was collected a day before transfection. The cells were inoculated in 24-well plates at a density of 1×10^5 cells per well after centrifugation and suspension. The transfections were performed with Lipofectamine 3000 (Invitrogen) as recommended by the manufacturer. DNA (1 μg) with 15 pmol miR-5134-5p was co-transfected into three wells. A double-luciferase reporter activity (GeneCopoeia) system was used to compare the activity of Renilla and dual-luciferase reporters 48 h after transfection.

miR-5134-5p Mimics/Inhibitor Transfection

Osteoblasts were transfected with miR-5134-5p mimics/inhibitors (Tsingke, China) at a final concentration of 10 nM using Lipofectamine RNAi transfection reagent (Beyotime, China) when they reached 60–70% confluent in the third passage. The cells were transfected in DMEM with 1 g/L glucose and 10% FBS at 37°C under 5% CO_2 for 24 h. After transfection, the media were changed to DMEM until harvest. Harvesting was performed according to the requirements of each specific assay, with the reported harvesting hours being the hours after transfection completion.

Real-Time Quantitative Reverse Polymerase Chain Reaction (qRT-PCR) Analysis

The gene expression levels were quantified using qRT-PCR. RNA was harvested using the cell/tissue Total RNA Kit (Yeason, China) and converted into cDNA using cDNA Synthesis SuperMix for quantitative PCR (qPCR) (Yeason, China). Micro RNA was harvested using a cell/tissue miRNA kit (Yeason, China) and converted into cDNA using the cDNA Synthesis SuperMix for qPCR (Yeason, China). Following this, real-time PCR was performed using SYBR green (Yeason, China) with the ABI StepOnePlus Real-Time PCR System (Applied Biosystems, Thermo Fisher Scientific Inc.) with specific primers. Glyceraldehyde 3-phosphate dehydrogenase (GAPDH) and U6 were selected as the loading control, and the $2^{-\Delta\Delta Ct}$ method was applied to calculate the relative expression. The experiments were performed in triplicate. The forward and reverse primers are listed in the subsequent section:

Forward, 5′-CACTCCCACCCTGAGATTTGT-3′,
Reverse, 5′-CCCCAGAGACATGATGAAGTCA-3′for TRAP;
Forward, 5′-CGGGTTTCAACGCCGACTA-3′,
Reverse, 5′-TTGGCACTAGAGACGGACAGA-3′for c-Fos;
Forward, 5′-GGAGAGTCCGAGAATCGAGAT-3′,
Reverse, 5′-TTGCAGCTAGGAAGTACGTCT-3′for Nuclear Factor Of Activated T Cells 1(NFATc1);[10]
Forward, 5′-GGACCATCTTTCTGCTCACTCTG-3′,
Reverse, 5′-GTTCACTACCTTATTGCCCTCCTG-3′for osteocalcin (OSC);
Forward, 5′-CCTTCAAGGTTGTAGCCCTC-3′,
Reverse, 5′-GGAGTAGTTCTCATCATTCCCG-3′for Runt-related transcription factor 2 (Runx2);
Forward, 5′-TCCATCGAAGAATCAAAGCAGAG-3′,
Reverse, 5′-CGAGAGTGTGGAAAGTGTGGAG-3′for Sialoprotein (Sia);
Forward, 5′-AGGAGGCACAAAGAAGCCATACG-3′,
Reverse, 5′-ATGCCTGCCTTGTACCACGAGC-3′for Osterix (Osx);
Forward, 5′-TCATTCCCACGTTTTCACATTC-3′,
Reverse, 5′-GTTGTTGTGAGCGTAATCTACC-3′for ALP;
Forward, 5′-GTGTGGAGATGTGCCGCTATGAC-3′,
Reverse, 5′-AGTCTCGGAGGTGCTCTTCAGTG-3′for JAK2;
Forward, 5′-TGTCAGATCACATGGGCTAAAT-3′,
Reverse, 5′-GGTCGATGATATTGTCTAGCCA-3′for STAT3;
Forward, 5′-CGCTCTTCTGTCTACTGAACTTCGG-3′,

Reverse, 5′-GTGGTTTGTGAGTGTGAGGGTCTG-3′for Tumor necrosis factor- α (TNF-α);
Forward, 5′-GGCCTAGCTCTGAGACAATGAAC-3′,
Reverse, 5′-TGACCTCAAACTTGGCAATACTC-3′for Interferon-γ (IFN-γ);
Forward, 5′-CACTACAGGCTCCGAGATGAACAAC-3′,
Reverse, 5′-TGTCGTTGCTTGGTTCTCCTTGTAC-3′for Interleukin-1beta (IL-1β);
Forward, 5′-GACTTCAACAGCAACTCCCAC-3′,
Reverse, 5′-TCCACCACCCTGTTGCTGTA-3′ for GAPDH.
Forward, 5′-CGACGGGTGGCCCTCTTT-3′,
Reverse, 5′-AGTGCAGGGTCCGAGGTATT-3′for miR-5134-5p;
Forward, 5′- CGCTTCGGCAGCACATATAC-3′,
Reverse, 5′- CACGAATTTGCGTGTCATCC-3′for U6;
RT Primer, 5′-GTCGTATCCAGTGCAGGGTCCGAGGTATTCGCACTGGATACG ACCTGCAG-3′.

Western Blot (WB)

A protein extraction reagent (Thermo, USA) was used, followed by centrifugation at 12,000 rpm for 15 min to isolate the protein from cells or exosomes. The protein concentration was determined using a bicinchoninic acid assay kit (Thermo, USA) before Western blotting. In the second step, the proteins were transferred onto 0.2 μm polyvinylidene difluoride membranes (Bio-Rad, USA) for 90 min at 300 mA. After blocking with 5% skim milk Tris-buffered saline with 0.1% Tween® 20 Detergent (FDbio, China) for 1 h, we probed the target protein by incubating the membranes overnight at 4°C with primary antibodies. Following this, a secondary antibody was incubated for an hour at room temperature on the membranes. The bands were visualised using an enhanced chemiluminescence kit (Fdbio, China), and the band densities were analysed using ImageJ. Matrix metallopeptidase 9 (MMP-9) (Abcam, USA), NFATc1 (Abcam, USA), Runx2 (Huabio, China), STAT3 (Huabio, China), phosphorylated (p)-STAT3 (Huabio, China), JAK2 (Huabio, China), p-JAK2 (CST, USA), CD9 (Abcam, USA), Alix (Huabio, China), CD63 (Abcam, USA), CD81 (Abcam, USA), and GAPDH (Proteintech, USA) were prepared using primary antibody dilution buffer (1:1000, Beyotime, China). Secondary antibodies (Yeason, China) were prepared using 5% skim milk (1:5000).

Model for Murine Periodontitis

Shanghai Slack Laboratory Animal Co., Ltd. (SCXK-2017-0005) provided the C57BL/6 mice (male, aged 6–8 weeks, 18–25g). Experimental animal ethics committee approval (2020-48, June 19, 2020) was obtained by the Second Affiliated Hospital of Zhejiang University for this study. The animal experiments were performed following Laboratory animal – Guidelines for ethical review of animal welfare (GBT 35892-2018).[17] There were five mice in one cage. All experimental animals were kept at a temperature of 20–26 °C, 40–70% of humidity, and 12 hours of alternating light. After being anesthetized by intraperitoneal injection of 1% pentobarbital, silk ligatures (5-0) were placed around the maxillary left second molars of the mice for 14 days to induce periodontitis. In this part of the experiment, we set up three experimental groups (BLANK: control group without any treatment. PBS: The upper left second molar of mice was ligated and injected with 10 μL PBS. OC-Exo: The upper left second molar of mice was ligated and injected with 10 μL OC-Exo with the concentration of 4 μg/μL). Each group had 8 mice. An injection of 10 μL of PBS or OC-Exo was administered at 0, 4, 8, and 12 days. All mice were sacrificed by cervical dislocation on day 14.

Micro-Computed Tomography (CT) Scanning and Reconstruction

The mice were euthanized with an overdose of pentobarbital sodium (intraperitoneal injection), following which maxillary alveolar bones were harvested. The harvested bones were then fixed with 4% paraformaldehyde and transferred to PBS. Further, a high-resolution micro CT scanner (Yxlon, Germany) was used for imaging examination. The micro CT parameters were as follows: integration time, 400 ms; voxel resolution, 16 μm; voltage, 50 kV; electrical current, 100 μA. Tissues with a CT value of >1500 Hu were defined as bone. Each scan was three-dimensional reconstructed and reoriented to the same position for analyzing the anatomical landmarks. Six predetermined sites on the buccal and

palatal surfaces were used to measure the distance between the cementoenamel junction and alveolar bone crest (CEJ-ABC distance). The area of observation in the transverse section was a circle with a fixed diameter between the mesial and distal roots of the second molar. The inter radicular regions of the maxillary second molars were selected to determine the bone volume per tissue volume (BV/TV).

Histology and Immunohistochemical(IHC) Analysis

Hematological analysis of the mice maxillae was performed using 4% paraformaldehyde. The samples were dehydrated after demineralizing and embedding in paraffin. Haematoxylin and eosin (H&E) staining was performed after the wax blocks were cut into sagittal sections measuring 3 μm. After immersion in ethylenediaminetetraacetic acid (pH 9.0) for 20 min, boiling, and washing with 1× PBS, the slide was incubated with the following primary antibodies: anti-tumour necrosis factor (TNF)-α (diluted 1:800; Huabio, China) and interferon (IFN)-γ (diluted 1:100; Huabio, China). The tissues were treated with secondary antibodies for 30 min at room temperature after incubation in a humidified tray for 24 h. Images of the histological sections were captured using a digital slice scanner (Vs200, Olympus).

Statistical Analysis

Means ± standard deviations are used to present the quantitative data. In the statistical analysis, we used SPSS 17.0 and GraphPad Prism 8.0 to perform an analysis of variance (ANOVA) and a least significant difference *t*-test. The differences between groups were analysed using a two-way ANOVA followed by a Bonferroni post hoc test. Statistical significance was set at $P < 0.05$. The experimental results obtained from the three repetitions were similar.

Results

Identification of Osteoclasts, Osteoblasts, and OC-Exo

The mononuclear macrophage RAW264.7 can differentiate into a multinuclear mature osteoclast in response to RANKL and after 5 days of treatment with 50 ng/mL RANKL-induced osteoclast differentiation. On treatment with RANKL, the TRAP-positive cell content significantly increased, as demonstrated by the TRAP staining graph (Figure 1A). NFATc1, c-Fos, and TRAP were detected using qRT-PCR (Figure 1B) as osteoclastogenesis-related genes. By inducing NFATc1 and MMP-9 protein expressions were significantly upregulated (Figure 1C).

Osteoblastic differentiation induction was achieved by treating osteoblasts with Ind for 5 days. An increase in the ALP activity (ALP staining) was observed in the presence of Ind during osteogenic differentiation (Figures 1D). And mineralisation in osteoblasts was observed by alizarin red staining after 14 days of induction (Figures 1E). OC, Runx2, and Sia mRNA expression levels were compared with those of the normal control (NC) (detected using qRT-PCR, Figure 1F). Based on Western blotting (Figure 1G), we observed that Ind significantly increased Runx2 protein expression.

The OC-Exos were isolated by ultracentrifugation from serum-free culture supernatants to determine their characteristics. OC-Exos had a diameter of 30–200 nm, as determined by nanoparticle tracking analysis (Figure 1H). TEM revealed that OC-Exos were round or round-like-shaped vesicles surrounded by a bilayer membrane of lipids (Figure 1I). Western blotting further revealed that the isolated vesicles expressed the exosomal markers Alix, CD63, CD81, and CD9 (Figure 1J).

OC-Exos Regulate the Differentiation of Osteoblastic Cells in vitro

OC-Exos labelled with PKH67 was incubated with osteoblasts for 12 h to demonstrate that it could be endocytosed, following which the images revealed a cytosolic distribution of PKH67-labelled OC-Exos (Figure 2A). In conclusion, osteoblasts efficiently absorbed exosomes extracted from osteoclasts.

In vitro, we examined how OC-Exos modulated osteoblastic differentiation to disrupt alveolar bone homeostasis. An osteoclastic-derived exosomal solution diluted on a per millilitre basis was added to the osteoblasts. A total of 20 μg/mL OC-Exos, 50 μg/mL OC-Exos, and 80 μg/mL OC-Exos were released into an induction medium, respectively. After 48 h of incubation, cell viability was determined using the CCK-8. After 5 days of incubation, Osx, Runx2, and ALP

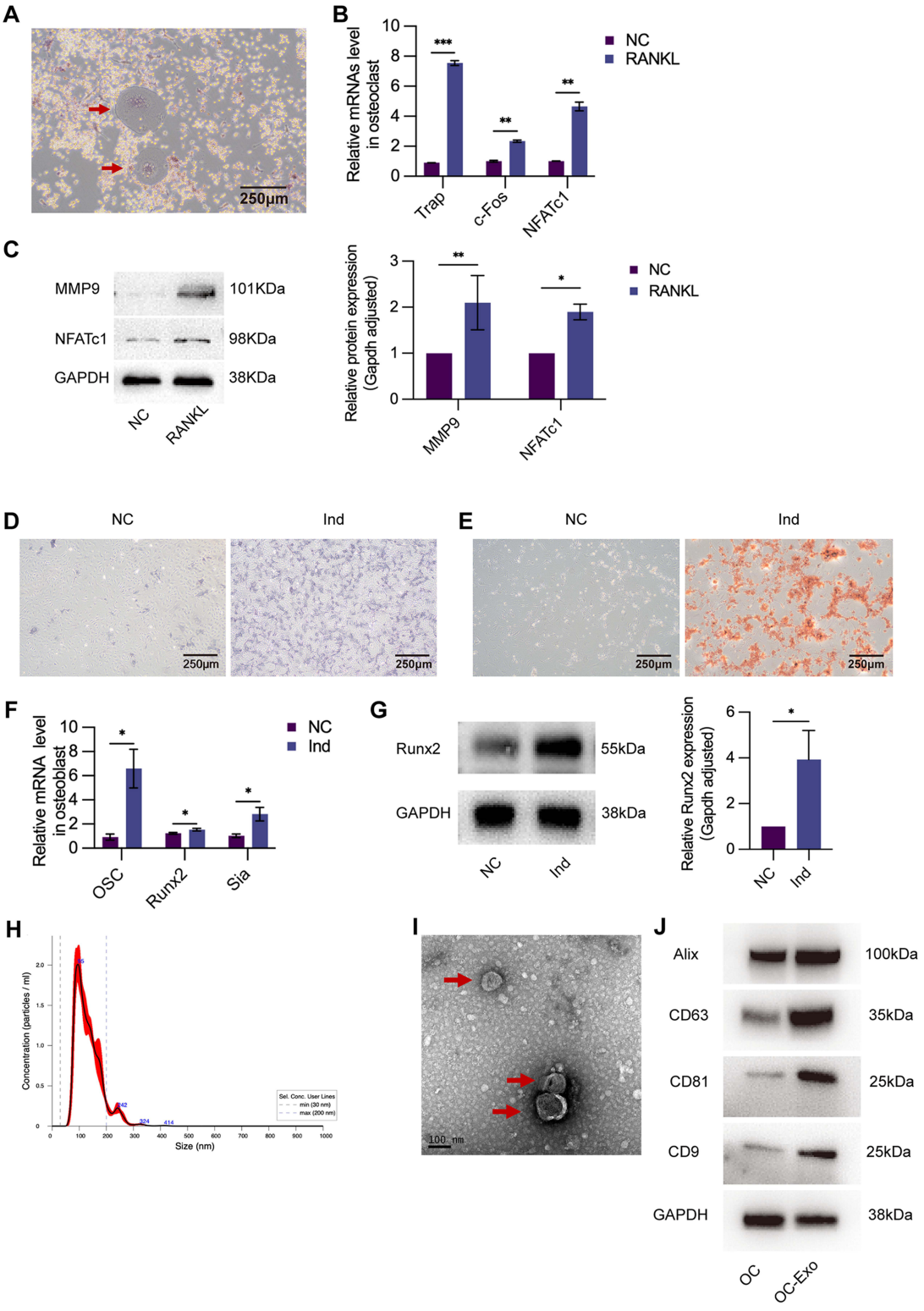

Figure 1 Characterization of osteoclast, osteoblast, and OC-Exo. (**A**) TRAP staining images showing TRAP-positive osteoclasts (40×) (indicated by the red arrowheads). (**B**) NC: control group without any treatment. RANKL: RAW264.7 treated with 50ng/mL RANKL. Compared with NC group, the relative expression of osteoclastic markers including TRAP, c-Fos, and NFATc1 were sharply increased in RANKL group. (**C**) WB revealed the proteins of MMP-9 and NFATc1 were enriched in RANKL group. (**D**) NC: control group without any treatment. Ind: osteoblastic cells cultured with osteogenic induction medium. ALP staining (40×) showed that Ind group (cultured with osteogenic induction medium) had higher alkaline phosphatase activity. (**E**) Alizarin red staining (40×) confirmed more calcium nodules and mature osteoblasts formation compared with NC group. (**F**) The relative expression of osteoblastic markers including OC, Runx2, and Sia were sharply increased in Ind group. (**G**) WB revealed the proteins of Runx-2 was enriched in Ind group. (**H**) NTA showed the size of particles was about 95nm. (**I**)OC-Exos were observed by Scanning electron microscopy (indicated by the red arrowheads). (**J**)WB showed the proteins of Alix, CD63, CD81, and CD9 were enriched in exosomes. *$p < 0.05$, **$p < 0.01$, ***$p < 0.001$.

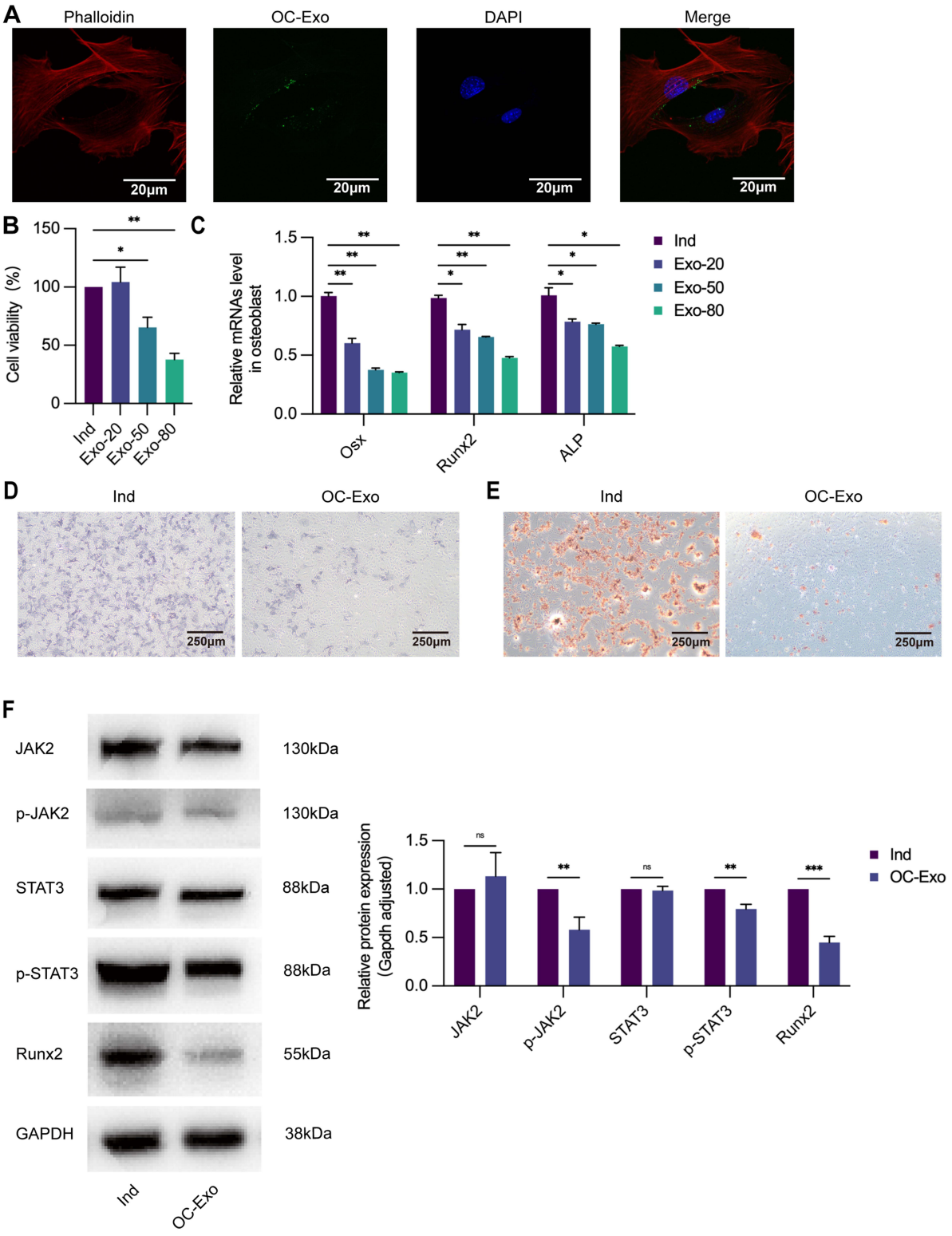

Figure 2 OC-Exos suppresses osteogenesis in vitro. (**A**) Exosomes derived from osteoclasts were labeled with green fluorescence PKH67 and co-cultured with osteoblastic cells respectively, green fluorescence represents exosomes in osteoblastic cells (600×). (**B**) Ind: osteoblastic cells cultured with osteogenic induction medium. Exo-20: osteoblastic cells treated with Ind and 20ug/mL OC-Exo. Exo-50: osteoblastic cells treated with Ind and 50ug/mL OC-Exo. Exo-80: osteoblastic cells treated with Ind and 80ug/mL OC-Exo. Cell viability of osteoblasts decreased with the increase of OC-Exo concentration following treatment by different concentrations of OC-Exos for 48h. (**C**) Osteogenesis-related genes were downregulated in OC-Exo-treated osteoblastic cells quantified by qRT-PCR analysis. (**D**) OC-Exo: osteoblastic cells treated with Ind and 20ug/mL OC-Exo. ALP staining (40×) reflected that OC-Exo decreased ALP activity and inhibited osteoblast differentiation. (**E**) Alizarin red staining (40×) confirmed less calcium nodules and mature osteoblasts formation compared with Ind group. (**F**) The level of osteoblastogenic-related protein p-JAK2, p-STAT3, and Runx2 were negatively correlated with the treatment of OC-Exos by WB. ns: no significant difference, *$p < 0.05$, **$p < 0.01$, ***$p < 0.001$.

expressions were determined using qRT-PCR. Based on concentration-dependence, compared with the Ind group, osteoblastic cell viability decreased (Figure 2B), and these gene expression levels significantly decreased in the OC-Exo group (Figure 2C). Meanwhile, we co-cultured 20 μg/mL OC-Exos with osteoblasts under the same conditions. OC-Exo-treated osteoblasts were cultured continuously for 5 days and assessed with ALP staining, which revealed a reduced osteogenic capability, to further determine the impact of OC-Exos on osteogenesis (Figure 2D). Similar results were obtained with Alizarin red when osteoblasts were treated with OC-Exos for 14 days (Figure 2E). A negative correlation was observed between the expression of osteoblastogenic-related proteins Runx2, p-JAK2, and p-STAT3 and treatment with OC-Exos (Figure 2F).

Exosomes from Osteoclasts Inhibit Osteoblastic Activity

Our study was performed using a Transwell system coated with polyethylene terephthalate membranes with 0.4-μm pores that allowed the transfer of exosomes (40-100 nm) but blocked most shed microvesicles and apoptotic bodies (>0.4 μm in diameter) to determine whether OC-Exos could inhibit osteoblastic activity. RAW264.7 cells were differentiated into osteoclasts after 50 ng/mL RANKL stimulation. We isolated primary osteoblast precursor cells from neonatal mice skulls and differentiated them in the osteogenic medium. GW4869 was used to reduce exosomes from osteoclasts.[18] The osteogenic capabilities were compared via ALP staining after co-culturing for 5 days and Alizarin red staining after co-culturing for 14 days (Figures 3A and B). Also, after co-culturing with osteoblasts for 5 days, they were harvested, and their proteins and RNA were extracted. qRT-PCR analysis revealed that Runx2, ALP, and Osx levels for osteoblasts in osteoblastic and osteoclastic co-cultures were significantly lower than those for osteoblasts in the Ind group (Figure 3C). The Runx2, p-JAK2, and p-STAT3 levels were further verified via Western blotting (Figure 3D). These relative indicators were significantly down-regulated in osteoblasts co-cultured with osteoclasts, while they were up-regulated after GW4869 treatment.

Analysis of the Functional Attributes Associated with the OC-Exos Gene Set and Signaling Pathway Changes

miRNA-sequencing analysis revealed differences in gene expression between OC-Exos and NC-Exos (exosomes from undifferentiated RAW264.7) that inhibited cell proliferation and osteogenic differentiation. OC-Exo up-regulated five targets and down-regulated three targets, and the results were illustrated using a heat map ($P < 0.05$, Figure 4A). As a result of the Gene Ontology enrichment analysis, miRNAs in OC-Exo are implicated in metabolic processes (Figure 4B). The Kyoto Encyclopaedia of Genes and Genomes pathway enrichment analysis was used to identify exosome-mediated gene expression (Figure 4C). Infectious diseases and environmental signal transduction were associated with genes related to them. The expression of miR-5134-5p in OC-Exo was significantly higher than that in NC group, as we discovered subsequently (Figure 4D). At the same time, we found that OC-Exos transport miR-5134-5p to osteoblasts. In a miRNA extraction experiment, osteoblasts were treated with 20 μg/mL, 50 μg/mL, or 80 μg/mL OC-Exos, and released into Ind (Figure 4E). It was observed that miR-5134-5p expression was up-regulated in a concentration-dependent manner compared with that in the Ind group.

Exosomal miR-5134-5p Regulates Osteogenic Differentiation Through the JAK2/STAT3 Signaling Pathway

Based on the data presented in Figure 5A, we speculated that miR-5134-5p might target JAK2. WT- and MUT-JAK2 were fused to luciferase and co-expressed with mus-miR-5134-5p mimics to verify this speculation. miR-5134-5p down-regulated WT-JAK2 expression but not MUT-JAK2 expression, suggesting that it was a direct target of JAK2 (Figure 5B).

The importance of the JAK2/STAT3 signaling pathway increases as osteoblastic differentiation increases. We first detected the transfection efficiency of miR-5134-5p mimics/inhibitors (Figure 5C) to verify the mechanisms of exosomal miR-5134-5p that inhibit osteogenic differentiation. At first, we revealed that miR-5134-5p mimics inhibit osteogenic differentiation while miR-5134-5p inhibitors promote it by ALP staining and Alizarin red staining (Figures 5D and E). To investigate the related genes which may be involved by miR-5134-5p including Runx2, ALP, JAK2, and STAT3, we used

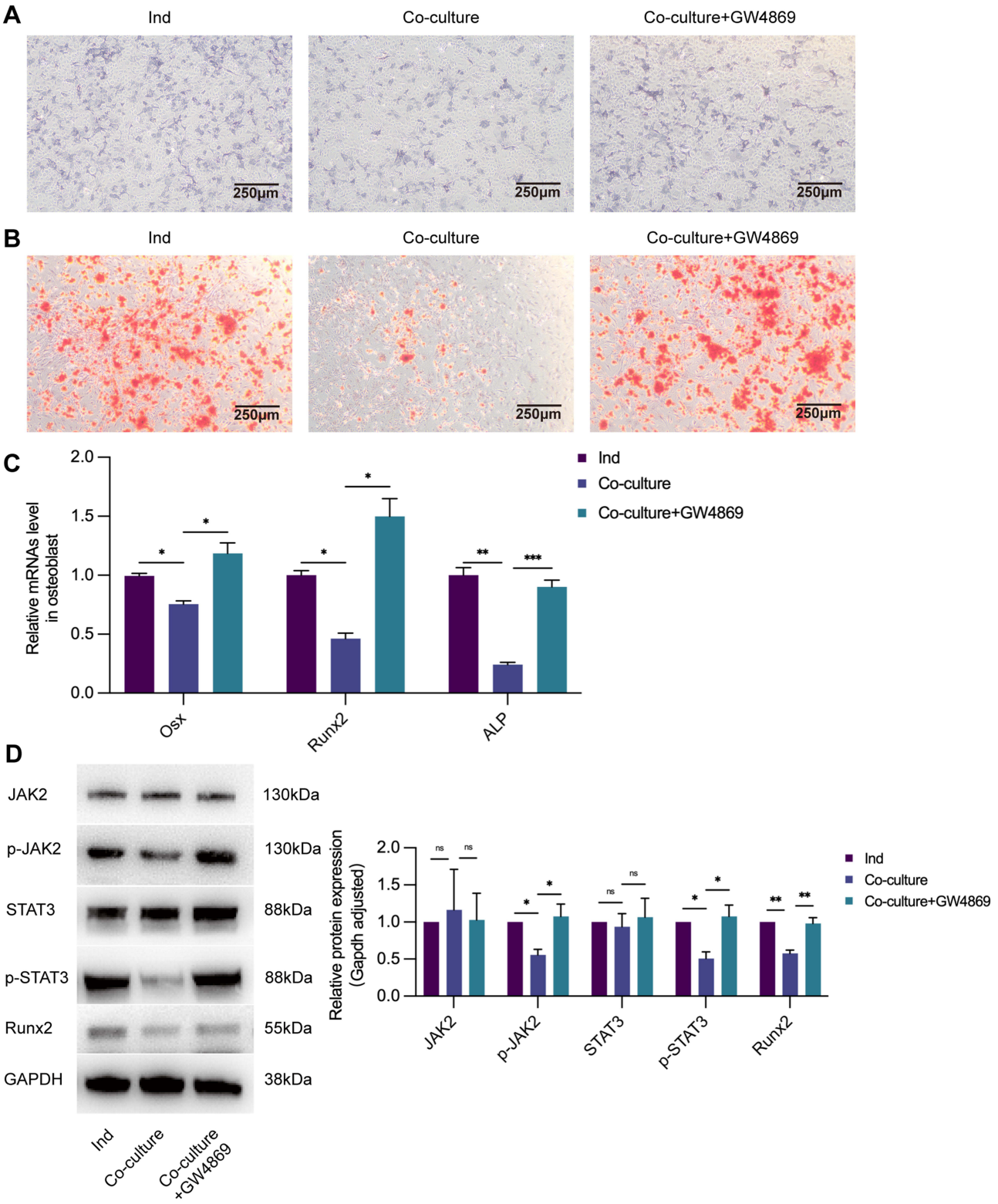

Figure 3 Exosomes from osteoclasts inhibit osteoblast activity. (**A**) Ind: osteoblastic cells cultured with osteogenic induction medium without being co-cultured with osteoclasts. Co-culture: osteoblastic cells in Transwell system. Co-culture+GW4869: osteoblastic cells in Transwell system, while osteoclasts in the upper chamber treated with exosomes inhibitor GW4869. Compared with Ind group, ALP staining (40×) showed that ALP activity was decreased in Co-culture group, while the effect could be promoted by GW4869. (**B**) Alizarin red staining (40×) confirmed less calcium nodules and mature osteoblasts formation than Ind group, while there were more calcium nodules and mature osteoblasts formation in Co-culture+GW4869 group. (**C**) The relative expression of osteogenesis-related genes Osx, Runx2, and ALP were downregulated in the Co-culture group and upregulated with the treatment of GW4869. (**D**) The level of osteoblastogenic-related protein p-JAK2, p-STAT3, and Runx2 were negatively correlated in the Co-culture group but positively correlated with GW4869 by WB. ns: no significant difference, $^{*}p < 0.05$, $^{**}p < 0.01$, $^{***}p < 0.001$.

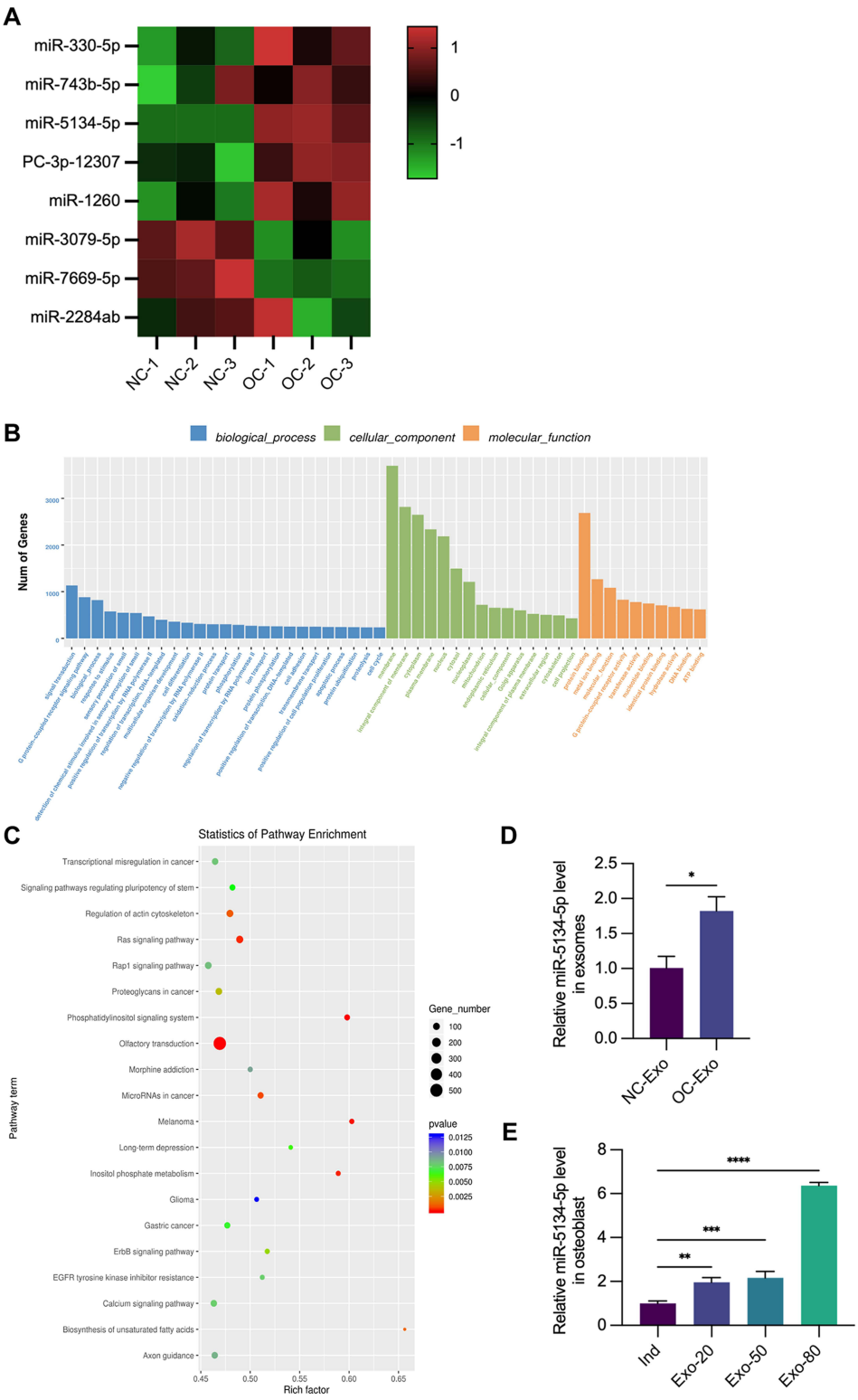

Figure 4 Analysis of functional attributes connected to OC-Exo changes in gene sets and signaling pathways. miRNA-seq comparison between the NC-Exo and OC-Exo groups. (**A**) NC: exosome from RAW264.7 without any treatment. OC: exosome from RAW264.7 treated with 50ng/mL RANKL. Heat map showed that compared with NC group, the expressions of miR-330-5p, miR-743b-5p, miR-5134-5p, PC-3p-12,307 and miR-1260 were up-regulated in OC group, while the expressions of miR-3079-5p, miR-7669-5p and miR-2284ab were down-regulated. (**B**) GO biological process classification of the genes. (**C**) KEGG enrichment analysis results were obtained by scatter plot. (**D**) Compared with NC-Exo group, the relative expression of miR-5134-5p was upregulated in the OC-exo group. (**E**) Ind: osteoblastic cells cultured with osteogenic induction medium. Exo-20: osteoblastic cells treated with Ind and 20ug/mL OC-Exo. Exo-50: osteoblastic cells treated with Ind and 50ug/mL OC-Exo. Exo-80: osteoblastic cells treated with Ind and 80ug/mL OC-Exo. Expression of miR-5134-5p in osteoblastic cells increased with the increase of OC-Exo concentration following treatment by different concentrations of OC-Exos. *$p < 0.05$, **$p < 0.01$, ***$p < 0.001$, ****$p < 0.0001$.

https://doi.org/10.2147/IJN.S413692 DovePress

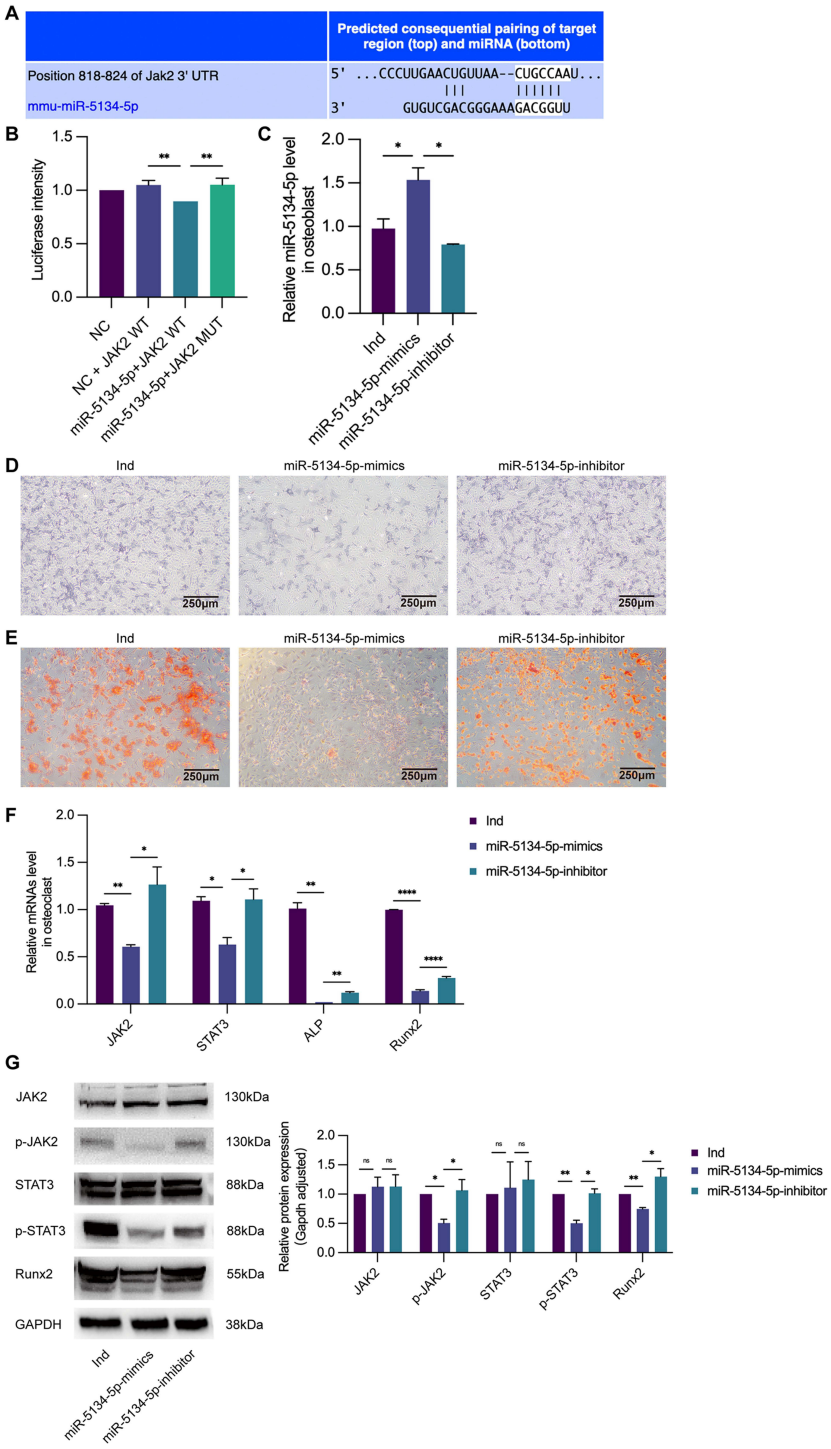

Figure 5 Exosomal miR-5134-5p regulates osteogenic differentiation through the JAK2/STAT3 signaling pathway. (**A**) We predicated the target of miR-5134-5p by using target gene prediction software. It showed that miR-5134-5p could regulate JAK2 by binding sites in the JAK2 3'UTR. (**B**) The dual-luciferase reporter assays. NC: MC3T3-E1 cells which were mock transfected. JAK2 WT: JAK2 wild type. JAK2 MUT: JAK2 mutant type. miR-5134-5p-mimics reduced the luciferase activity compared with NC+ JAK2 WT group and miR-5134-5p+JAK2 MUT group. (**C**) Ind: untransfected osteoblastic cells cultured with osteogenic induction medium. miR-5134-5p-mimics: osteoblastic cells transfected by miR-5134-5p-mimics. miR-5134-5p-inhibitor: osteoblastic cells transfected by miR-5134-5p- inhibitor. Compared with Ind group, expression of miR-5134-5p in osteoblastic cells increased in miR-5134-5p-mimics group, while the effect could be inhibited by miR-5134-5p-inhibitor. (**D**) ALP staining (40×) showed that ALP activity was decreased in miR-5134-5p-mimics and increased in miR-5134-5p-inhibitor group. (**E**) Alizarin red staining (40×) confirmed less calcium nodules and mature osteoblasts formation in miR-5134-5p-mimics group than Ind group, while there were more calcium nodules and mature osteoblasts formation in miR-5134-5p-inhibitor group. (**F**) The relative expression of genes in the JAK2/STAT3 signaling pathway JAK2, STAT3, Runx2, and ALP were downregulated in the miR-5134-5p-mimics group and upregulated in the miR-5134-5p-inhibitor group. (**G**) The level of protein p-JAK2, p-STAT3, and Runx2 were negatively correlated in the miR-5134-5p-mimics group but positively correlated in the miR-5134-5p-inhibitor group by WB. ns: no significant difference, $*p < 0.05$, $**p < 0.01$, $****p < 0.0001$.

qRT-PCR and Western blotting techniques. The results revealed that miR-5134-5p mimics reduced JAK2 and STAT3 expression, whereas miR-5134-5p inhibitors increased JAK2/STAT3 expression (Figure 5F). Western blotting was used to further confirm the JAK2 and STAT3 phosphorylation levels. miR-5134-5p mimics down-regulated p-JAK2, p-STAT3, and Runx2 expressions, whereas miR-5134-5p inhibitors showed the opposite trend (Figure 5G).

OC-Exos Accelerated Alveolar Bone Resorption in Mice with Periodontitis

Ligatures were used to induce periodontitis to evaluate the effects of OC-Exos in mice with periodontitis. In the periodontitis group, mice were injected with 10 μL of PBS or 4 μg/μL of OC-Exos in the left maxillary buccal mucosa on days 0, 4, 8, and 12. The mice were euthanized on day 14. Periodontitis-induced alveolar bone resorption was measured using micro CT. In OC-Exo-treated mice, alveolar bone resorption and the CEJ-ABC distance significantly increased (Figure 6A and B), while the BV/TV decreased (Figure 6C). Additionally, we harvested mRNA from the maxilla for qRT-PCR and stained maxilla samples with H&E post-OC-Exo treatment. In the OC-Exo group, TNF-α, IFN-γ, and interleukin-1β levels were significantly higher than those in the PBS group (Figure 6D). H&E staining showed that the gingival papilla in OC-Exo group and PBS group was severely damaged, the epithelial pegs rete pegs were elongated, the fiber cells in lamina propria were disordered, and a large number of inflammatory infiltrates. Compared with PBS group, gingival tissue destruction was more severe in OC-Exo group (Figure 6E). Besides, IHC staining revealed that TNF-α and IFN-γ expressions in the maxillary tissue of the OC-Exo group was significantly higher than that in the PBS-treated mice group (Figure 6F). Furthermore, TRAP staining revealed that TRAP expression significantly increased in the maxillary tissues of the OC-Exo group, indicating lesser osteoclastic lineage (Figure 6G).

Discussion

Osteoclast-osteoblast imbalance owing to periodontitis results in gradual alveolar bone destruction that cannot be easily repaired or replaced.[19,20] In this study, we concentrated on the molecular mechanisms of osteogenic differentiation mediated by OC-Exos. Based on our results, we concluded that OC-Exos could transduce miR-5134-5p into osteoblasts. Due to its increased expression, miR-5134-5p inhibited the JAK2/STAT3 pathway, negatively regulated osteogenic differentiation, and accelerated periodontitis progression.

Exosomes are extracellular vesicles with a size of 40–100 nm that originate from endocytosis and are secreted by various cells in the extracellular matrix for paracrine signaling and communication.[21] Yang et al[22] extracted exosomes from RANKL-induced RAW 264.7 cells and observed their sizes at 50–100 nm under transmission electron microscopy. In our study, exosomes from osteoclasts were extracted by transmission electron microscopy, with diameters of about 50–100 nm. NTA results also showed that the main particle size of extracted exosomes was concentrated at 95nm, suggesting that the vesicles obtained by superfast centrifugation were indeed exosomes.

In chronic periodontitis, alveolar bone resorption could be attributed to the disruption of the balance between osteoclast bone resorption and osteoblast bone formation.[2] Studies have reported that bone-related cells, such as osteoblasts, osteocytes, and bone marrow mesenchymal stem cells, could release exosomes containing active molecules to regulate the homeostasis of bone metabolism.[23–25] Sun et al[26] reported that OC-Exos could penetrate osteoblasts through their surface ligand ephrinA2 binding to the osteoblast surface receptor ephrin type-A receptor 2, releasing important biological information and mobilizing osteoblast signaling molecules to inhibit osteoblastic proliferation and differentiation. Yang et al[22] also reported the inhibitory effect of OC-Exos on osteoblast differentiation. As previously demonstrated, OC-Exos disrupt the information exchange between osteoblasts and osteoclasts, negatively regulating osteoblastic proliferation and differentiation, thereby increasing alveolar bone resorption. We labelled OC-Exos with PKH67 to investigate whether OC-Exos are transferable to osteoblasts and observed that osteoblastic cytoplasm contained exosomes with fluorescence. In addition, we observed that OC-Exos diminish osteoblastic proliferative viability and Runx2 expression, a marker of osteoblastic differentiation. A similar result was obtained with Alizarin red staining, indicating that OC-Exos could invade osteoblasts and inhibit growth and differentiation. We co-cultured osteoclasts with osteoblasts in a Transwell system and treated them with GW4869 to disrupt exosomal production as an additional measure to verify exosomal function.[27,28] Consequently, Runx2, ALP, and Osx mRNA expressions were down-regulated in the co-culture model. As a result of ALP and Alizarin red staining, osteoblastic differentiation was

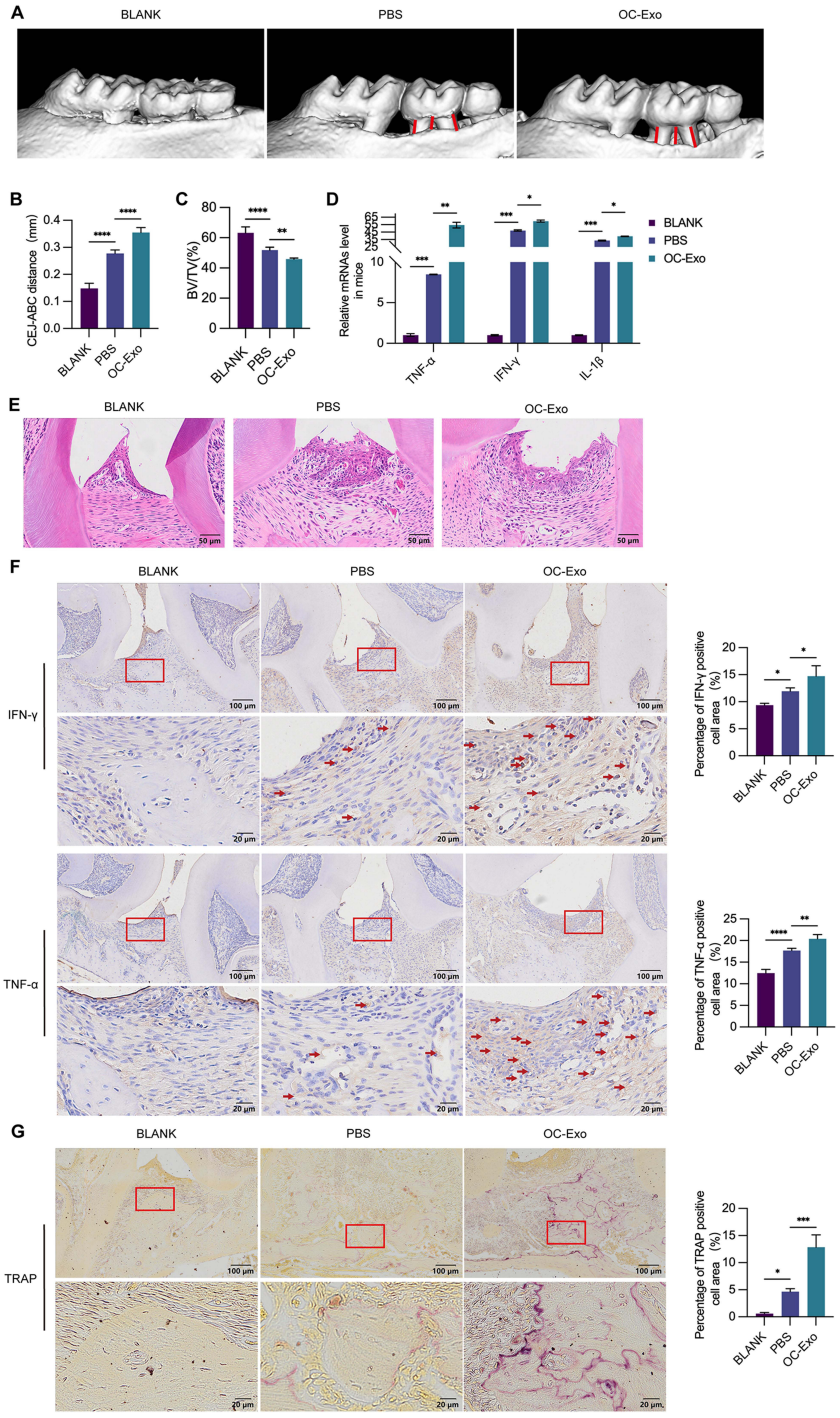

Figure 6 OC-Exos accelerated alveolar bone resorption in mice with periodontitis. (**A**) BLANK: control group without any treatment. PBS: The upper left second molar of mice was ligated and injected with 10 μL PBS. OC-Exo: The upper left second molar of mice was ligated and injected with 10 μL OC-Exo with the concentration of 4 μg/μL. 3D reconstructed images produced by micro-CT were performed on maxillae of Blank, PBS, and OC-Exo groups (The red line represents CEJ-ABC, the upper end is the cement-enamel junction and the lower end is the alveolar bone crest). (**B**) The average distance of CEJ-ABC on three palatal sides (mesial, central, and distal sites) and three buccal sides (mesial, central, and distal sites) of the left maxillary second molar was measured. Data are shown as means ± SEM. Compared with BLANK group, the distance of CEJ-ABC in PBS group was significantly increased, while the distance of CEJ-ABC in OC-Exo group was significantly higher than that in PBS group. (**C**) Compared with BLANK group, bone volume per tissue volume (BV/TV) analysis in PBS group was significantly decreased, while BV/TV in OC-Exo group was significantly lower than that in PBS group. (**D**) The expression of genes associated with inflammatory including TNF-α, IFN-γ, and IL-1β were significantly up-regulated in OC-Exo group. (**E**) H&E staining images showed that periodontal tissue inflammation in OC-Exo group was more serious than that in PBS group. (**F**) Immunohistochemical analysis showing the expression level of TNF-α and IFN-γ increased in OC-Exo group compared with PBS group (red arrowheads indicated positive cell, red frames indicate the positions of higher-magnification images). (**G**)TRAP staining images showed trap staining showed that the number and activity of mature osteoclasts in OC-Exo group were increased than those in PBS group. *$p < 0.05$, **$p < 0.01$, ***$p < 0.001$, ****$p < 0.0001$.

also compromised compared with that of the Ind group; however, GW4869 reversed this inhibitory effect. Overall, our results suggest that osteoblast-derived exosomes could inhibit bone formation when transferred to osteoblasts.

Extracellular vesicles, such as exosomes, which are separated from the plasma membrane and protect miRNA from RNase-induced degradation, could be used to transport miRNA across cells.[29–31] Li et al[32] reported down-regulation of ALP, osteopontin, osteocalcin, and bone sialoprotein when miR-214 overexpressed exosomes from differentiated mouse bone marrow-derived macrophages were applied to osteoblast-like cells. We demonstrated for the first time that mature OC-Exos were highly expressed by miR-5134-5p, and elevated miR-5134-5p expression was also observed in osteoblasts co-cultured with OC-Exos, suggesting that the exosome miR-5134-5p is transferred from osteoclasts to osteoblasts and mediates communication between them. Similarly, Yang et al[22] indicated that OC-Exos could carry and deliver miR-23a-5p into osteoblasts, which could effectively suppress osteogenic differentiation by inhibiting Runx2 and promoting YAP1-mediated MT1DP. Despite this, no previous research had examined the function of miR-5134-5p. We searched the National Centre for Biotechnology Information database (https://www.ncbi.nlm.nih.gov/gene/100628603) to learn more about miR-5134-5p. miR-5134-5p regulates gene expression post-transcriptionally in multicellular organisms as a result of its effect on mRNA stability and translation. Hence, we inspected the target mRNA of miR-5134-5p on the TargetScan website and identified JAK2 as a potential target. JAK2/STAT3 signaling activation plays a crucial role in promoting osteoblastic proliferation and differentiation by regulating osteobiology.[33,34] Upon cytokines binding to receptors of tyrosine kinase, they form ligand-receptor complexes and immediately trigger the phosphorylation of JAK.[35] By phosphorylating tyrosine sites on JAK, Stat3 will dock with the SH2 structural domain for phosphorylation modifications. As Stat3 gets phosphorylated, it gets translocated to the nucleus, binding to genes and regulating transcription.[36,37] As humans develop their skeletal systems, growth hormone inhibits Runx2 transcriptional activity by interacting with Stat3 and Runx2,[38] suggesting that JAK2/STAT3 may be a pivotal trigger for the differentiation process of osteoblasts. According to Yu et al,[39] inhibiting JAK2/STAT3 signaling inhibited the osteogenic proliferation of bone marrow stem cells and impaired bone healing. In the present study, we confirmed the binding site between OC-Exo-derived miR-5134-5p and JAK2 by luciferase assays and the regulation's negative effect of miR-5134-5p on p-JAK2 and p-STAT3 expression was then verified in vitro. Our experimental results also demonstrated the Runx2, p-JAK2, and p-STAT3 down-regulation in osteoblasts with OC-Exo intervention. In accordance with this, miR-5134-5p derived from OC-Exos could inhibit osteoblastic differentiation via the JAK2/STAT3 axis, thereby regulating bone formation.

In mice with periodontitis, H&E staining, IHC staining of TNF-α and IFN-γ, and micro-CT revealed that OC-Exo treatment further aggravated periodontal inflammation and accelerated alveolar bone resorption. Wang et al[40] reported that circulating exosome levels were two-fold higher in mice with lipopolysaccharide (LPS)-induced bone loss. Besides, LPS-induced exosomal increase inhibited osteoblast formation in MC3T3-E1 cells in vitro. These results further proof that OC-Exos play a crucial role in the communication between osteoclasts and osteoblasts in periodontitis-induced bone resorption.

Osteoblastic differentiation plays a considerable role in alveolar bone regeneration, arising from several intersecting causes.[41] Firstly, we observed that OC-Exos inhibited osteoblastic proliferation and differentiation. Moreover, we observed that miR-5134-5p expression increased in OC-Exos and that this miRNA negatively regulated osteogenic differentiation by inhibiting the JAK2/STAT3 axis. miR-5134-5p negatively affected osteoblastic differentiation when it was transferred into the cells. Similarly, exosomes isolated from osteoclasts (OC-Exos) accelerated alveolar resorption in vivo. Several mechanisms have been reported to mediate the osteogenic differentiation of osteoblasts, with the JAK2/STAT3 axis being one of the most important axes.[33,34] As reported in the present study, miR-5134-5p targets JAK2, indicating a mechanistic role for miR-5134-5p in osteoblastic differentiation. When up-regulated, JAK2 can no longer suppress osteoblastic differentiation of osteoblasts. However, no relevant reports on specific functional studies of miR-5134-5p as a target in periodontitis progression exist, and further research is warranted. Furthermore, the current research on exosomes is very extensive. Apart from exosome-loaded bioinformatics substances, exosomes are also available and widely used in gene editing and nanodrug delivery.[42–44] Nevertheless, there are still many uncertainties in the study of nanocarriers, and further research is needed.

Conclusions

Overall, our study findings indicate that OC-Exos promote alveolar resorption by inhibiting osteoblastic differentiation in vitro and in vivo. In this negative effect, miR-5134-5p, which is enriched in OC-Exos, inhibits osteogenic differentiation by suppressing

JAK2/STAT3 axis activation and might play a crucial role. Therefore, our findings suggest that therapeutic inhibition of miR-5134-5p in osteoclasts might serve as an effective bone anabolic strategy to relieve periodontitis and re-establish bone homeostasis.

Data Sharing Statement

The data presented in this study are openly available in GEO database (GSE222004).

Ethical Approval

The animal study protocol was approved by the Ethics Committee of The Second Affiliated Hospital of Zhejiang University (2020-48, June 19, 2020).

Acknowledgments

Our sincere thanks go out to everyone who helped us write this dissertation. It is our great pleasure to acknowledge the help we have received from our supervisors, Dr Tan and Professor Chen, who have provided us with valuable suggestions during our academic studies. And it has been a great pleasure to receive inspiration and guidance from them throughout the preparation of this thesis. Without their patient instruction, insightful criticism and expert guidance, the completion of this thesis would not have been possible.

Author Contributions

All authors made a significant contribution to the work reported, whether that is in the conception, study design, execution, acquisition of data, analysis and interpretation, or in all these areas; took part in drafting, revising or critically reviewing the article; gave final approval of the version to be published; have agreed on the journal to which the article has been submitted; and agree to be accountable for all aspects of the work.

Funding

This work was supported by the National Natural Science Foundation of China (81800972, 82170954) and Medical Healthy Scientific Technology Project of Zhejiang Province (grant numbers 2022498513).

Disclosure

The authors declare that the research was conducted in the absence of any commercial or financial relationships that could be construed as a potential conflict of interest.

References

1. Henderson B, Kaiser F. Bacterial modulators of bone remodeling in the periodontal pocket. *Periodontol*. 2018;76(1):97–108. doi:10.1111/prd.12160
2. Sims NA, Martin TJ. Coupling the activities of bone formation and resorption: a multitude of signals within the basic multicellular unit. *Bonekey Rep*. 2014;3:481. doi:10.1038/bonekey.2013.215
3. Hu CH, Sui BD, Liu J, et al. Sympathetic neurostress drives osteoblastic exosomal MiR-21 transfer to disrupt bone homeostasis and promote osteopenia. *Small Methods*. 2022;6(3):e2100763. doi:10.1002/smtd.202100763
4. Wang Q, Shen X, Chen Y, Chen J, Li Y. Osteoblasts-derived exosomes regulate osteoclast differentiation through miR-503-3p/Hpse axis. *Acta Histochem*. 2021;123(7):151790. doi:10.1016/j.acthis.2021.151790
5. Wang W, Qiao SC, Wu XB, et al. Circ_0008542 in osteoblast exosomes promotes osteoclast-induced bone resorption through m6A methylation. *Cell Death Dis*. 2021;12(7):628.
6. Aass KR, Nedal TMV, Tryggestad SS, et al. Paired miRNA-and messenger RNA-sequencing identifies novel miRNA-mRNA interactions in multiple myeloma. *Sci Rep*. 2022;12(1):12147.
7. Movassagh M, Morton SU, Hehnly C, et al. mirTarRnaSeq: an R/bioconductor statistical package for miRNA-mRNA target identification and interaction analysis. *BMC Genom*. 2022;23(1):439.
8. Leng Q, Chen L, Lv Y. RNA-based scaffolds for bone regeneration: application and mechanisms of mRNA, miRNA and siRNA. *Theranostics*. 2020;10(7):3190–3205.
9. Coutinho de Almeida R, Ramos YFM, Mahfouz A, et al. RNA sequencing data integration reveals an miRNA interactome of osteoarthritis cartilage. *Ann Rheum Dis*. 2019;78(2):270–277.
10. Jing W, Feng L, Peng K, Zhang W, Wang B. Formononetin attenuates osteoclast differentiation and calcium loss by mediating transcription factor AP-1 in type I diabetic mice. *J Biochem Mol Toxicol*. 2022;36(6):e23042. doi:10.1002/jbt.23042

11. Mousavi SM, Amin Mahdian SM, Ebrahimi MS, et al. Microfluidics for detection of exosomes and microRNAs in cancer: state of the art. *Mol Ther Nucleic Acids*. 2022;28:758–791. doi:10.1016/j.omtn.2022.04.011
12. Ghaemmaghami AB, Mahjoubin-Tehran M, Movahedpour A, et al. Role of exosomes in malignant glioma: microRNAs and proteins in pathogenesis and diagnosis. *Cell Commun Signal*. 2020;18(1):120. doi:10.1186/s12964-020-00623-9
13. Lv PY, Gao PF, Tian GJ, et al. Osteocyte-derived exosomes induced by mechanical strain promote human periodontal ligament stem cell proliferation and osteogenic differentiation via the miR-181b-5p/PTEN/AKT signaling pathway. *Stem Cell Res Ther*. 2020;11(1):295. doi:10.1186/s13287-020-01815-3
14. Damerau A, Gaber T, Ohrndorf S, Hoff P. JAK/STAT activation: a general mechanism for bone development, homeostasis, and regeneration. *Int J Mol Sci*. 2020;21(23):9004. doi:10.3390/ijms21239004
15. Sanpaolo ER, Rotondo C, Cici D, Corrado A, Cantatore FP. JAK/STAT pathway and molecular mechanism in bone remodeling. *Mol Biol Rep*. 2020;47(11):9087–9096. doi:10.1007/s11033-020-05910-9
16. Liu B, Lu Y, Wang Y, Ge L, Zhai N, Han J. A protocol for isolation and identification and comparative characterization of primary osteoblasts from mouse and rat calvaria. *Cell Tissue Bank*. 2019;20(2):173–182. doi:10.1007/s10561-019-09751-0
17. MacArthur Clark JA, Sun D. Guidelines for the ethical review of laboratory animal welfare People's Republic of China National Standard GB/T 35892-2018 [Issued 6 February 2018 Effective from 1 September 2018]. *Anim Models Exp Med*. 2020;3(1):103–113. doi:10.1002/ame2.12111
18. Peng Y, Zhao M, Hu Y, et al. Blockade of exosome generation by GW4869 inhibits the education of M2 macrophages in prostate cancer. *BMC Immunol*. 2022;23(1):37. doi:10.1186/s12865-022-00514-3
19. Hajishengallis G, Korostoff JM. Revisiting the Page & Schroeder model: the good, the bad and the unknowns in the periodontal host response 40 years later. *Periodontol*. 2017;75(1):116–151.
20. Li Y, Ling J, Jiang Q. Inflammasomes in alveolar bone loss. *Front Immunol*. 2021;12:691013. doi:10.3389/fimmu.2021.691013
21. Norouzi-Barough L, Shirian S, Gorji A, Sadeghi M. Therapeutic potential of mesenchymal stem cell-derived exosomes as a cell-free therapy approach for the treatment of skin, bone, and cartilage defects. *Connect Tissue Res*. 2022;63(2):83–96. doi:10.1080/03008207.2021.1887855
22. Yang JX, Xie P, Li YS, Wen T, Yang XC. Osteoclast-derived miR-23a-5p-containing exosomes inhibit osteogenic differentiation by regulating Runx2. *Cell Signal*. 2020;70:109504. doi:10.1016/j.cellsig.2019.109504
23. Cappariello A, Loftus A, Muraca M, Maurizi A, Rucci N, Teti A. Osteoblast-derived extracellular vesicles are biological tools for the delivery of active molecules to bone. *J Bone Mineral Res*. 2018;33(3):517–533. doi:10.1002/jbmr.3332
24. Morrell AE, Brown GN, Robinson ST, et al. Mechanically induced Ca(2+) oscillations in osteocytes release extracellular vesicles and enhance bone formation. *Bone Res*. 2018;6:6. doi:10.1038/s41413-018-0007-x
25. Hu H, Wang D, Li L, Yin H, He G, Zhang Y. Role of microRNA-335 carried by bone marrow mesenchymal stem cells-derived extracellular vesicles in bone fracture recovery. *Cell Death Dis*. 2021;12(2):156. doi:10.1038/s41419-021-03430-3
26. Sun W, Zhao C, Li Y, et al. Osteoclast-derived microRNA-containing exosomes selectively inhibit osteoblast activity. *Cell Discov*. 2016;2:16015. doi:10.1038/celldisc.2016.15
27. Xia X, Zhang L, Wu H, et al. CagA(+) helicobacter pylori, not CagA(-) Helicobacter pylori, infection impairs endothelial function through exosomes-mediated ROS formation. *Front Cardiovasc Med*. 2022;9:881372. doi:10.3389/fcvm.2022.881372
28. Wang H, Qi Y, Lan Z, et al. Exosomal PD-L1 confers chemoresistance and promotes tumorigenic properties in esophageal cancer cells via upregulating STAT3/miR-21. *Gene Ther*. 2023;30(1–2):88–100. doi:10.1038/s41434-022-00331-8
29. Mullen M, Williams K, LaRocca T, et al. Mechanical strain drives exosome production, function, and miRNA cargo in C2C12 muscle progenitor cells. *J Orthopaed Res*. 2023;41(6):1186–1197. doi:10.1002/jor.25467
30. Yao P, Lu Y, Cai Z, et al. Research progress of exosome-loaded miRNA in osteosarcoma. *Cancer Control*. 2022;29:10732748221076683. doi:10.1177/10732748221076683
31. Zeng ZL, Xie H. Mesenchymal stem cell-derived extracellular vesicles: a possible therapeutic strategy for orthopaedic diseases: a narrative review. *Biomater Transl*. 2022;3(3):175–187. doi:10.12336/biomatertransl.2022.03.002
32. Li D, Liu J, Guo B, et al. Osteoclast-derived exosomal miR-214-3p inhibits osteoblastic bone formation. *Nat Commun*. 2016;7:10872. doi:10.1038/ncomms10872
33. Hou X, Tian F. STAT3-mediated osteogenesis and osteoclastogenesis in osteoporosis. *Cell Commun Signal*. 2022;20(1):112. doi:10.1186/s12964-022-00924-1
34. Jo S, Wang SE, Lee YL, et al. IL-17A induces osteoblast differentiation by activating JAK2/STAT3 in ankylosing spondylitis. *Arthritis Res Ther*. 2018;20(1):115.
35. Bharadwaj U, Kasembeli MM, Robinson P, Tweardy DJ. Targeting janus kinases and signal transducer and activator of transcription 3 to treat inflammation, fibrosis, and cancer: rationale, progress, and caution. *Pharmacol Rev*. 2020;72(2):486–526. doi:10.1124/pr.119.018440
36. Johnson DE, O'Keefe RA, Grandis JR. Targeting the IL-6/JAK/STAT3 signalling axis in cancer. *Nat Rev*. 2018;15(4):234–248. doi:10.1038/nrclinonc.2018.8
37. Li J, Yin Z, Huang B, Xu K, Su J. Stat3 signaling pathway: a future therapeutic target for bone-related diseases. *Front Pharmacol*. 2022;13:897539. doi:10.3389/fphar.2022.897539
38. Ziros PG, Georgakopoulos T, Habeos I, Basdra EK, Papavassiliou AG. Growth hormone attenuates the transcriptional activity of Runx2 by facilitating its physical association with Stat3beta. *J Bone Mineral Res*. 2004;19(11):1892–1904. doi:10.1359/JBMR.040701
39. Yu X, Li Z, Wan Q, et al. Inhibition of JAK2/STAT3 signaling suppresses bone marrow stromal cells proliferation and osteogenic differentiation, and impairs bone defect healing. *Biol Chem*. 2018;399(11):1313–1323. doi:10.1515/hsz-2018-0253
40. Wang Y, Zhang L, Wang K, et al. Circulating exosomes from mice with LPS-induced bone loss inhibit osteoblast differentiation. *Calcif Tissue Int*. 2022;111(2):185–195. doi:10.1007/s00223-022-00977-x
41. Huang X, Xie M, Xie Y, et al. The roles of osteocytes in alveolar bone destruction in periodontitis. *J Transl Med*. 2020;18(1):479. doi:10.1186/s12967-020-02664-7
42. Guo H, Huang X. Engineered exosomes for future gene-editing therapy. *Biomater Transl*. 2022;3(4):240–242. doi:10.12336/biomatertransl.2022.04.003
43. Zhou D, Zhou F, Sheng S, Wei Y, Chen X, Su J. Intra-articular nanodrug delivery strategies for treating osteoarthritis. *Drug Discov Today*. 2023;28(3):103482. doi:10.1016/j.drudis.2022.103482
44. Guo J, Wang F, Hu Y, et al. Exosome-based bone-targeting drug delivery alleviates impaired osteoblastic bone formation and bone loss in inflammatory bowel diseases. *Cell Rep Med*. 2023;4(1):100881. doi:10.1016/j.xcrm.2022.100881